JOURNAL OF MATERIALS SCIENCE 33 (1998) 1679–1698

Review
Reinforced cast metals
Part I *Solidification microstructure*

R. ASTHANA
Manufacturing Engineering, Technology Department, University of Wisconsin-Stout, Menomonie, WI 54751, USA
E-mail: asthanar@uwstout.edu

The solidification process in fibre- and particle-reinforced metals is modified due to solute screening, thermal shielding, heterogeneous nucleation, fluid damping, particle pushing and morphological instabilities at the liquid–solid–fibre boundary. These factors lead to considerable variations in grain size, grain morphology, microsegregation and macrosegregation, and reinforcement distribution in the matrix. This article examines the roles of the above factors in the evolution of solidification microstructure in composites under controlled growth as well as under normal casting conditions. © *1998 Chapman & Hall*

1. Introduction

While metal–matrix composites such as cast graphite–aluminium attracted the attention of the materials community as early as the 1930s [1], major developments of industrial importance in the metal–matrix area took place during the last three decades. Innovations in processing science and materials design, and the development of a variety of inexpensive reinforcements led to the growth of the engineered materials field. Liquid-phase fabrication of composite materials using solidification and casting techniques has long been considered economically viable owing primarily to the low viscosity of liquid metals, net-shape manufacturing capability of casting processes, and flexibility in designing the structure by controlled solidification. Table I gives a partial listing of liquid-phase composite fabrication methods; the basic principles of various fabrication techniques have been discussed in [2]. It is conceivable that the presence of an insoluble second phase (reinforcement) in a liquid metal will modify the basic heat, mass and momentum transport phenomena during liquid-to-solid transformation. Thus, the reinforcement can serve as a barrier to diffusion of heat and solute, can catalyse the heterogeneous nucleation of phases crystallizing from the melt, can restrict fluid convection and can induce morphological instabilities in the growth front by imposing curvature on the contact perimeter with the solidification front. As a result, the matrix solidification response is altered. While the fibre architecture in engineering preforms could be prohibitively complex, the solidification zone is relatively uniform in preforms of directional aligned fibres. This permits quantitative treatment of solidification morphology and solute segregation during controlled solidification. This paper presents a non-mathematical review of the following microstructural features of fibre- and particulate-reinforced cast composites: the composition and morphology of directionally solidified composites, and the principal observations on structure evolution in pressure-cast, spray-formed, *in-situ*-grown and other composites. The nucleation and growth phenomena and the factors influencing the microscopic distribution of particulates are also covered. Interfaces, which constitute another important structural feature of composites, are discussed separately in Part II of this series.

2. Solute segregation

A reinforcement in a solidifying alloy obstructs the diffusion of solute away from the phase change interface [3–9]. The resulting solute build-up in the gap between the solidification front and the reinforcement reduces the solute gradient at the growth front. When an initially planar interface approaches a diffusion barrier, the motion of the interface segment nearest the barrier is retarded relative to the rest of the interface. This induces a curvature in the front which, in turn, leads to lateral solute currents, which further enhance the curvature and lead to a steeper solute gradient in the liquid at the leading interface region. As a result, a planar interface becomes unstable and breaks down into a cellular and, finally, a dendritic interface. Once a dendritic structure forms within interfibre channels, coarsening of secondary dendrite arms takes place. Coarsening takes place by ripening, coalescence and solid-state diffusion in a manner similar to unreinforced metals; however, the presence of fibres modifies the kinetics of the processes involved.

TABLE I Partial listing of liquid-phase techniques with selected examples

Infiltration techniques	Slurry techniques		*In-situ* techniques	Spray techniques	Combinations
	Mixing	Casting			
Vacuum infiltration SiC–Al, W–Cu, Al_2O_3–(Al–Li) Al_2O_3–(Al, Mg), suction-casting	*Injection* C–Al, Al_2O_3–(Mg, Al)	*Sand* SiC, C, Al_2O_3 zircon, mica in Al alloys	*Self-infiltration* DIMOX, PRIMEX of Lanxide for Al, Zn metal–matrix composites	*Solid–liquid* *liquid–gas* *liquid–liquid*	*Powder extrusion + squeeze casting* SiC and C in Al and Mg
Pressure infiltration C, Al_2O_3, SiC in Al, Mg Cu, Zn and intermetallics	*Impeller* (Fully liquid) C, SiC, Al_2O_3, mica, glass in Al alloys (Semisolid) $Al_{23}O_3$, SiC in Al alloys	*Permanent mould* SiC, Al_2O_3, mica in Al alloys	*Solvent based* XD process TiB_2–Al, TiC–Al	Al_2O_3–Cu, W–Cu, TiC–Fe, SiC–Al, borides, silicides in metals, intermetallics	*Cold press + casting* Al_2O_3–Al
Squeeze casting Al_2O_3, SiC, C, glass hybrids in Al, Mg, Cu, Sn and Zn	*Magnetohydrodynamics* (Semisolid) Al_2O_3, SiC in Al and Mg alloys	*Centrifugal* SiC, zircon, mica, graphite in Al	*Directional solidification* NbC–Co, TaC–Co, Ni–Al(–Cr), Ni–Al(–Me), sapphire–NiAl		*Infiltration + hot isostatic pressing* Al_2O_3–$TiAl_2$
Centrifugal infiltration C microballoons, Al_2O_3 in Al and Sn alloys	*Ultrasonic* Oxides, borides, carbide in Al, Sn, Fe and Pb alloys	*Full mould* C–Al, SiC–Al	*Combustion synthesis* TiC–Al		
Lorentz force Al_2O_3–Al	*Mix alloy* Dispersion strengthened alloys, metal-matrix composites	*Investment* Al_2O_3–Al, SiC–Al intermetallic matrix composites			
Infrared Al_2O_3, SiC in Al, intermetallic matrix composites		*Squeeze casting* (*pre-mix*) SiC–Al, SiC–Zn, C–Al			
Reactive SiC–C–Si, TiC–Al, Al_2O_3–Al_2O_3–NiAl		*Die casting* C–Al, Al_2O_3 in Al, Mg and Zn			
		Continuous casting SiC–Al			

The fibres impose a curvature in the growth front at its boundary in contact with the fibres (contact angle, $\theta > 90^\circ$) and assist coalescence of dendrite arms [7, 9]. For a growth front with a finite curvature, the liquid composition at the interface under equilibrium conditions is given by the Gibbs–Thompson relationship. When the front curvature varies spatially along the latter's surface, e.g., in the case of a dendritic front, the interfacial concentration becomes a function of the position. As a result, lateral solute gradients develop and the diffusion of solute down these gradients determines the rate of coarsening. Ripening (i.e., remelting of small dendrite arms and resolidification onto larger arms) usually occurs at low solid volume fractions (i.e., early during solidification) whereas coalescence occurs predominantly at high solid volume fractions. With continued growth, when the scale of the microstructure becomes comparable with interfibre spacing, ripening ceases and coarsening occurs by dendrite arm coalescence. The coarsening of secondary dendrite arms by solid-state diffusion is enhanced in composites owing to the small size of the diffusion zone between closely spaced fibres. As a result, microsegregation in composite is reduced compared with that in the unreinforced alloy.

Fig. 1 shows the influence of interfibre spacing on solute segregation in an alumina–(Al–Cu) composite. When the secondary dendrite arm spacing (DAS) is smaller than the interfibre spacing (Fig. 1a, case 1), the fibres do not influence the matrix solidification behaviour and normal coring patterns are observed (Fig. 1b). When the scale of the matrix microstructure is comparable with the interfibre spacing (Fig. 1c), the secondary phases (e.g., eutectic) are deposited onto the fibre surface. Microprobe scans across the interfibre regions of the matrix indicate that solute content is highest at the fibre surface and smallest in the centre of interfibre regions. Finally, when the interfibre spacing is smaller than the secondary DAS (which can be controlled by the rate of external heat extraction), the segregation is reduced and less secondary phase is precipitated from the matrix (Fig. 1d). Under these conditions, the solute content in the matrix is higher than in the unreinforced matrix.

For a given geometry of the interfibre channel, the secondary dendrite arms would be completely

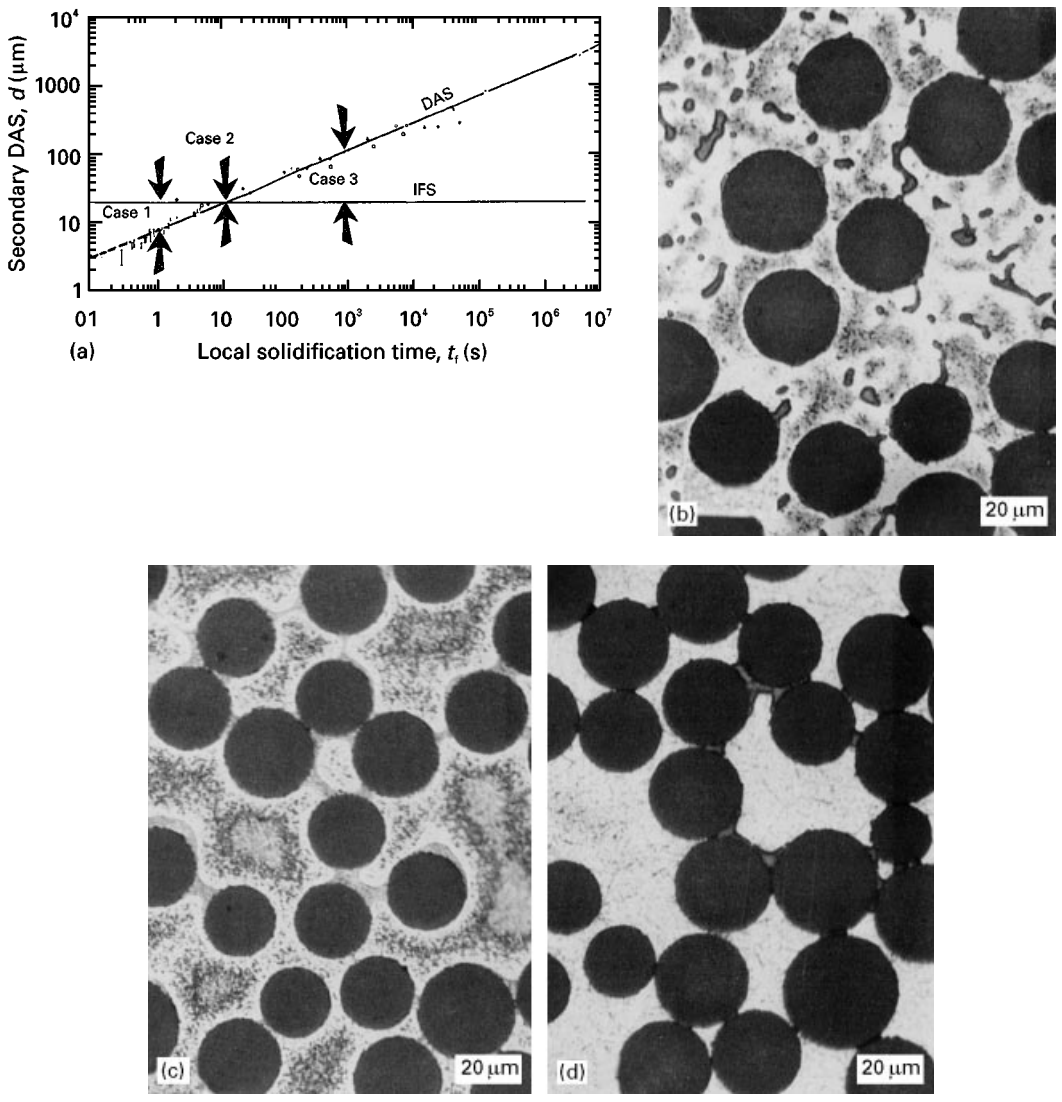

Figure 1 Structure formation in alumina-fiber-reinforced Al–4.5 wt % Cu composite: (a) dependence of the primary-phase morphology and second-phase distribution on the relative magnitudes of secondary DAS and interfibre spacing; (b) microstructure for case 1 in (a); (c) microstructure for case 2 in (a); (d) microstructure for case 3 in (a) [9].

eliminated after some critical time, t_c, during solidification. Experiments have shown [9] that this critical time, t_c, increases roughly linearly with increasing total solidification time, t_f. For times $t < t_c$, the structure is dendritic whereas, for $t_c < t < t_f$, solidification takes place in a non-dendritic fashion. Thus the magnitude of the critical time t_c relative to t_f determines the degree of dendritic character of the cast microstructure; if t_c is reached early during solidification (t_c/t_f small), then the microstructure becomes increasingly non-dendritic in character, with solute isoconcentrates becoming everywhere parallel to the fibre–matrix interface. If, for a given type of interstice, t_f is sufficiently small to satisfy the condition $t_f < t_c$, then fibres would not influence the dendritic microstructure of the reinforced matrix. The condition $t_c = t_f$ gives the *minimum* solidification time, t_f, which would yield a fully coalesced microstructure in a given type of interstice. The critical time can be theoretically predicted in terms of solidification parameters and alloy properties.

The interfibre channels in composites exhibit a higher minimum solute concentration than the unreinforced alloy [9]; this minimum solute concentration increases with a decrease in the channel size and increase in solidification time, t_f. Thus, within the smallest interfibre channels and at long solidification times, the minimum solute concentration would increase markedly. The minimum solute concentration is a measure of microsegregation and can be calculated within topologically symmetrical interfibre channels [9] on the basis of a model of moving-boundary diffusion-controlled growth in a finite domain. As microsegregation in composites is reduced, the best way to homogenize the microstructure without the need for additional heat treatment is to cool the composite at a moderate rate to the solidus temperature and to hold it there to coalesce the dendritic microstructures and to erase all microsegregation [9].

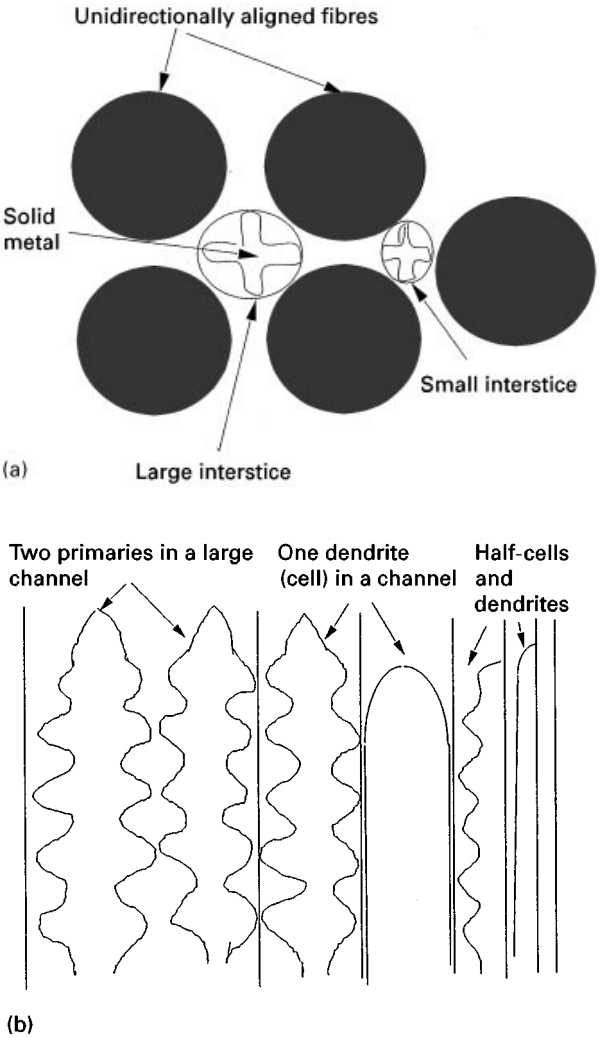

Figure 2 Schematic diagrams showing (a) constrained solidification in the interfibre regions of fibre-reinforced composites [12] and (b) modulation of solidification morphology as a function of interfibre spacing [6].

3. Solidification morphology

As the reinforcement restricts the solute transport processes by diffusion and flow, the solidification morphology is altered when the interfibre channels become sufficiently small (Fig. 2a). Transparent models show that the interface morphology changes from dendritic to cellular to nearly planar as the channel width decreases. The parameter D/V (D is the diffusion coefficient, and V the growth velocity) governs the solute field interaction distance. Also, as the contact angle at the triple-phase junction (solid–liquid–fibre) is seldom 90°, a finite non-zero curvature is imposed at the three-phase junction which destabilizes the planar front in very narrow channels.

The cell tip undercooling is determined by the longitudinal solute gradient in the intercellular region. The tip undercooling is slightly increased for cylindrical cells, growing concentrically at steady state within cylindrical interstices when the cell radius is reduced to half its unconstrained spacing [10]. When the interstice diameter is reduced to below 10% of the unconstrained cell size, higher undercoolings are achieved. However, the representation of a single cell centrally positioned within an interstice is a geometric oversimplification; off-centred cells grow into half-cells along one side of the interstice with the solid contacting the fibre along that side [5, 6]. The geometry of the channel is important too; growth in cylindrical capillaries results in cells that are larger and have a lower tip undercooling compared with cellular growth within flat parallel plates. In real composites, the solidification morphology and compositions vary over a wide range owing to variations in fibre size and channel geometry (converging and diverging fibres, parallel fibres, and high-aspect-ratio platelets and whiskers). The width of the interfibre channel may not be constant over the entire length of the fibres [5]; as a result, heat flow and solute fields change significantly. Under steady-state growth, a variable cross-section alters the interface velocity which, in turn, modifies the morphology of the growth front in the region of changed cross-section. Microsegregation is also altered compared with the case of a channel of constant cross-section. When the changed cross-section is much larger than the primary arm spacing, there is a very small effect on dendrite

spacing. On the other hand, low growth velocities and large cross-section changes lead to drastic changes in the microstructure; for example, a planar interface may break into cellular interface and then into a dendritic interface. As the growth front approaches a progressively narrowing region, fluid flow occurs to compensate for the volume contraction. Significant fluid flow can reduce the local solute gradient at the interface, thus allowing the interface to freeze at a higher temperature, which will cause it to accelerate.

It is conceivable that the range of perturbation wavelengths for morphological instability in the growth front will be restricted by the interfibre spacing [6, 7, 9, 10]. The critical wavelength for plane front stability in fibre-reinforced composites is larger than the interfibre spacings of engineering preforms; the fibres, therefore, tend to stabilize the plane front by restricting the growth of critical perturbations. At much larger interfibre spacings (large enough to accommodate a decade of critical wavelengths), the plane-front-to-cellular transition remains uninfluenced by the fibres. However, near the contact perimeter of the fibre with the front, the amplitude of perturbation increases more rapidly than along the rest of the plane front at the onset of instability because of the surface tension effect.

In the dendritic growth regime, interstices of diameter significantly smaller than primary DAS inhibit formation of secondary arms and increase the propensity for cellular solidification (Fig. 2b). Under these conditions, cellular or half-cellular growth morphologies form [6]. Repeated interactions between the solute diffusion field and the reinforcement cause oscillatory motion of the interface and lead to cellular growth under conditions where dendrites normally form in the unreinforced alloy. Conversely, when the channel width is slightly larger than the cell spacing for cellular growth near the cell–dendrite transition, dendrites are favoured over cells. At very small G/V values, a dendritic structure develops in composites even when the interstice diameter is significantly smaller than the primary arm spacing in the unreinforced alloy. While no significant increase in dendrite tip undercooling occurs owing to spatial constraints, the dendrites are irregular and ill defined, and have contorted secondary arms. Typically, an ill-defined dendritic structure is observed when the interfibre spacing is smaller than the DAS in the unreinforced alloy by a factor of rougly two [11]. Regions with interfibre spacing larger than twice the DAS show a dendritic structure and the normal extensive coring. As the reinforcement enhances the coalescence of dendrite arms, the average secondary DAS at a given total solidification time is more in the composite than in the unreinforced alloy. The relationship between secondary dendrite arm spacing, λ, of the unreinforced alloy and solidification time, t, for Al–4.5 wt% Cu alloy is [12] $\lambda = 7.5\ t^{0.89}$ whereas for the Al_2O_3–fibre (55%)-reinforced Al–4.5 wt% Cu alloy, the relationship is of the form $\lambda = 9.7\ t^{0.51}$ (the higher temporal exponent for the composite indicates more rapid coarsening).

As the reinforcement constitutes physical barrier to solute diffusion, the solid grows from the centres of interfibre channels, and avoids the fibres. As a result, the reinforcement is surrounded by the last freezing eutectic liquid and solute-depleted regions in composites are usually found in the centre of interfibre spacings whereas the fibre surfaces are enriched in solute and secondary phase (the discontinuously reinforced composites show a similar behaviour although the geometry of the solidification zone is highly irregular). As most commercial ceramic fibres in common matrices (Al, Mg and Zn alloys) do not catalyse the heterogeneous nucleation of the primary solid, the matrix grain size in composites is not reduced by the fibres. However, there are exceptions to this behaviour and heterogenous nucleation together with grain refinement occurs in systems such as Al–Cu alloy reinforced with sintered TiC; in this case, α-Al nucleates on the TiC surface. Likewise, primary silicon nucleates heterogeneously on the ceramic reinforcement in hypereutectic Al–Si alloys.

The association of fibres with the last freezing colonies could, in theory, be caused by various mechanisms. It has been proposed that thermal effects play an important role in altering solute segregation [13–15]. Ceramic fibres used as reinforcement in metals usually have a lower thermal diffusivity and a higher heat capacity than the matrix metal does and may be expected to cool more slowly than the matrix and to be slightly warmer. The liquid on their surface would then be last to solidify. Small but finite temperature differences could exist between the two during sufficiently rapid solidification. These temperature differences may be large enough to influence solidification on a microscopic scale. Other possibilities such as localized displacement (pushing) of fibres by the growth front and formation of microvoid due to thermal expansion mismatch (where the residual melt may be sucked during cooldown) also have been suggested but are likely to be of lesser importance. For alloy solidification, the long-range solute interactions are probably the most important factors in determining the segregation of solutes on the reinforcement surface.

4. Processing effects on composite microstructure

4.1. Pressure-cast composites

The solidification microstructures of pressure-cast fibre-reinforced metals are modified primarily owing to the thermodynamic depression of the phase change temperature and increased undercooling (Clausius effect), and the elastic compression, deformation and relaxation of the preform in the presence of solidification [16–19]. The application of pressure increases the fibre volume fraction in localized areas; as a result, the size of the solidification zone is reduced in the compressed portion of the preform whereas it is increased in the fibre-impoverished regions. This results in an uneven fibre distribution and an inhomogeneous matrix structure. While fibre segregation can be minimized at relatively high initial fibre volume fractions (Fig. 3), fibre-to-fibre contact and metal-starved cavities may be difficult to avoid. Preform compression is

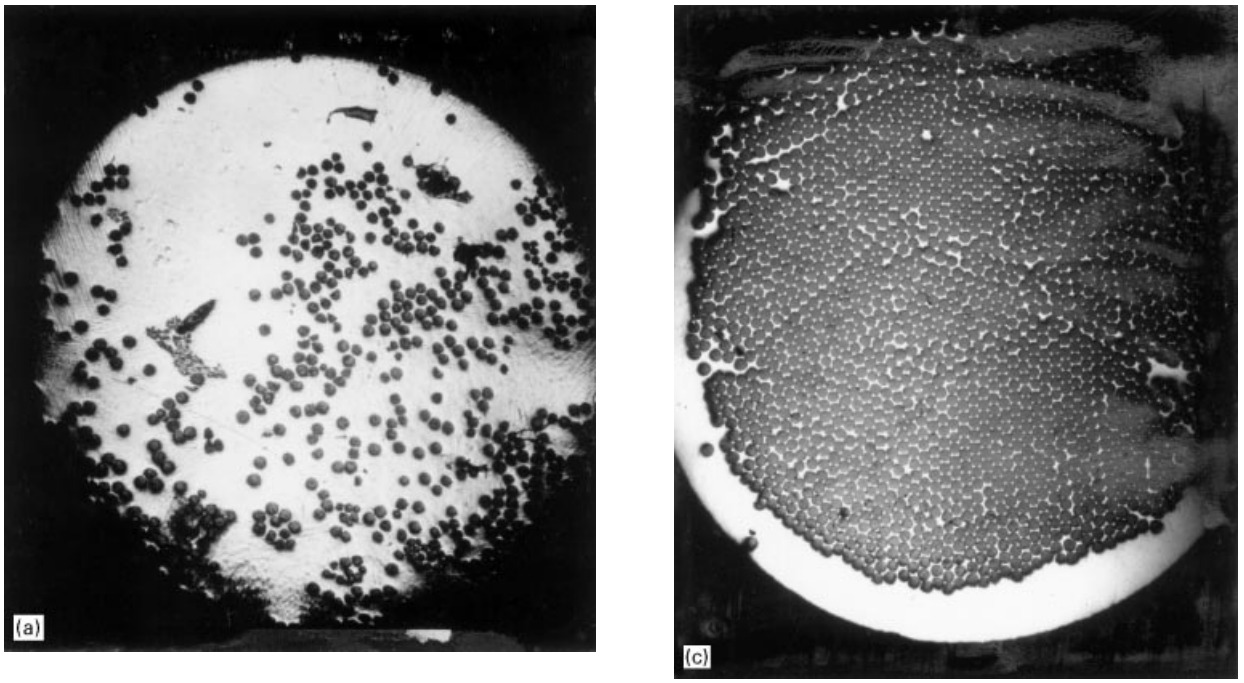

Figure 3 Transverse views of pressure-cast sapphire-fibre-reinforced Ni-base superalloy composites with unidirectionally aligned fibres showing the influence of initial fibre volume fraction on the fibre distribution [20].

enhanced by lower fibre pre-heat temperatures which enhance metal viscosity and increase the hydrodynamic pressure of metal on the preform. If infiltration is appreciably faster than solidification, then the preform is fully infiltrated first, followed by flow cessation and elimination of hydrodynamic drag; the preform can then elastically relax before appreciable solidification from external cooling has progressed. However, if solid metal forms in the composite casting prior to complete elastic recovery of the preform, the relaxation of the preform to its original shape and size is inhibited. This results in an increase in the average fibre volume fraction in the reinforced portion of the casting.

Preform compression and associated changes in the fibre volume fraction alter the solute profiles [17] because of restricted solute transport by bulk convection. Because the preform is able to relax only in solid-impoverished zones, more metal of nominal solute content will flow through the pores in relatively less densely packed regions compared with regions where solidification inhibits preform relaxation. A step drop usually occurs in the fibre volume fraction in going from the segregated regions, to regions having the nominal solute concentration. At relatively low preform temperatures, full relaxation of the preform occurs in regions of nominal solute concentrations. On the other hand, at high initial preform temperatures the viscous drag on the preform is relatively small but fibres near the wall are cooled relatively rapidly and assist localized solidification of the metal near the die walls. While both laboratory-scale and industrial castings show these microstructural features, qualitative differences exist between the two that are important in process scale-up. For example, the fibre-reinforced castings made under industrial die-casting conditions exhibit [17] fine equiaxed grain structure which extends in the casting to distances well beyond the fibre-enriched and solute-segregated regions. Such large equiaxed regions are normally not observed in laboratory trials where the infiltration rates and preform compression are small. This is because the high infiltration rates in industrial die casting disperse small primary metal nuclei formed initially on the fibre surface to larger distances where they refine the grain structure.

Besides macrodefects that form owing to fibre segregation, chemical interactions between fibre and matrix lead to fibre poisoning, grain coarsening in the fibre, and fibre weakening due to brittle reaction products and notch formation. Thus, in pressure-cast NiAl- and Fe_3Al-matrix composites reinforced with zirconia containing PRD 166 (alumina) fibres, the

high fabrication temperatures result in fibre grain growth [19] whereby the zirconia particles are swept by migrating grain boundaries to the fibre surface in contact with the melt. This contact leads to zirconia's dissolution and generation of free zirconium by a reduction reaction with the metal. Later, during solidification, the zirconium concentration increases to a point where it reduces the alumina of the fibre and forms zirconia again.

As pressure casting can incorporate high fibre volume fractions in the metal, solidification is severely constrained and the structural length scales greatly altered. For example, a high fibre volume fraction leads to a fine DAS. Thus, in pressure-cast Zn–Al alloys reinforced with alumina (Saffil) fibres, the average DAS was reduced from about 30 μm for the unreinforced matrix to 20 μm and 15 μm for the 10% and 20% fibre volume fractions, respectively. Still finer dendrites are formed in composites containing 27% fibre volume fractions [21]. When the reinforcement is not spatially constrained by either binders or a woven preform architecture, considerable spatial redistribution and preferred reorientation of the reinforcement can take place owing to the high fluid shear of pressure casting [22]. Likewise, matrix solutes also are redistributed by fluid convection under pressure.

4.2. *In-situ* composites

Relatively clean reinforcement–matrix interfaces and a spatially uniform distribution of very fine (and often single-crystal) reinforcement characterize the microstructure of *in-situ*-grown composites. The *in-situ* composite growth techniques include the various liquid–gas, liquid–solid, liquid–liquid and mixed salt reactions. Lanxide's DIMOX and PRIMEX processes [23–26], Martin-Marrietta's Exothermic Dispersion (XD^{TM}) process [27, 28], directional solidification of eutectics and monotectics, reactive infiltration, reactive spray forming, and combustion synthesis (also called self-propagating high-temperature synthesis (SHS)). Among the earliest *in-situ* composites were the directional solidified eutectics, and the most recent composites include metal- and ceramic-matrix composites fabricated using the SHS and reactive spray forming.

Controlled directional solidification of eutectics yields a dual-phase structure (Fig. 4a) in which one of the phases grows as fibres or platelets. The geometry, size and spacing of the second phase is controlled by controlling the cooling rate and temperature gradient. A pre-cast ingot of a eutectic alloy is melted and traversed in a steep temperature gradient at a controlled rate in order to grow the reinforcement. The directional solidification process creates dual-phase structures with some toughening potential, and preferred alignment of grain boundaries for applications (e.g., turbine blades) where directional stresses could cause grain-boundary creep and deformation. High-temperature *in-situ* composites such as Ni–TiC and Co–TiC for aircraft engine applications are grown by directional solidification. These materials display excellent high-temperature strength, creep resistance and thermal stability.

In Lanxide's pressureless infiltration process (DIMOX and PRIMEX) to make *in-situ* composites, oxidation of molten Al at temperatures in excess of 1200 K produces a continuous Al_2O_3 matrix with an interpenetrating three-dimensional network of metal microchannels. The growth of this "composite-matrix" into preforms consisting of reinforcing particles or fibres produces three interpenetrating phases: the preform, the reaction product and the unreacted metal. Alloying Al with Mg or Zn produces metastable surface oxides during composite growth which inhibit passivation of the melt and control the supply of oxygen at the reaction interface, thereby permitting continued "wicking" of metal through microchannels towards the growth front. Thus, the reaction front is fed by the flow of molten metal via microchannels in the porous oxide, and by the dissolution of metastable surface oxides. Structural refinement during growth can be achieved by adding a suitable alloying element, e.g., addition of Ni to the parent alloy in the case of AlN–Al ceramic composites refines the structure.

The microstructure development during composite growth by Lanxide's DIMOX process is characterized by four separate stages [23–25] (Fig. 4b). The first stage consists of initial melting and superheating of the Al–Mg alloy to 1123–1173 K, together with the formation of hemispherical cap on the solid. The surface oxidation of melt at these temperatures forms a duplex layer of magnesium oxide (MgO) and magnesium spinel ($MgAl_2O_4$) that contains a fine dispersion of metallic inclusions. The second stage consists of gradual thickening of this duplex layer as the temperature is further raised to 1373–1573 K. In this stage the oxidation kinetics are severely retarded and a near-zero growth rate is attained. The surface in contact with air gets coated with a thin (about 10 μm) layer of MgO whereas a thicker (about 50 μm) layer of $MgAl_2O_4$ forms between the MgO and the parent alloy. In the third stage, metal wicked through pores and microcracks in the MgO–$MgAl_2O_4$ layer speads over the duplex layer and forms small nodules of oxide–metal composite. These composite nodules then undergo rapid lateral growth (the fourth stage) and coalesce to form a macroscopically planar growth front which continues to grow until the entire alloy is consumed or processing is discontinued. The growth is controlled by the dissolution of a MgO surface layer by a thin underlying layer of molten alloy, from where alumina precipitates epitaxially on the existing oxide. Thus, a dissolution–precipitation mechanism controls the composite's growth. The dissolution rate of surface layer of MgO is a function of alloy composition and is controlled by liquid metal diffusion and flow through the composite microchannels.

The formation of microporosity due to solidification shrinkage at high temperatures and/or large particle sizes, and loss of toughness due to brittle phases formed as a result of excessive oxidation of the metal are common defects in Lanxide composites. While a change in the matrix alloy chemistry may limit the formation of brittle intermetallic phases, only limited freedom may be exercised in the selection of

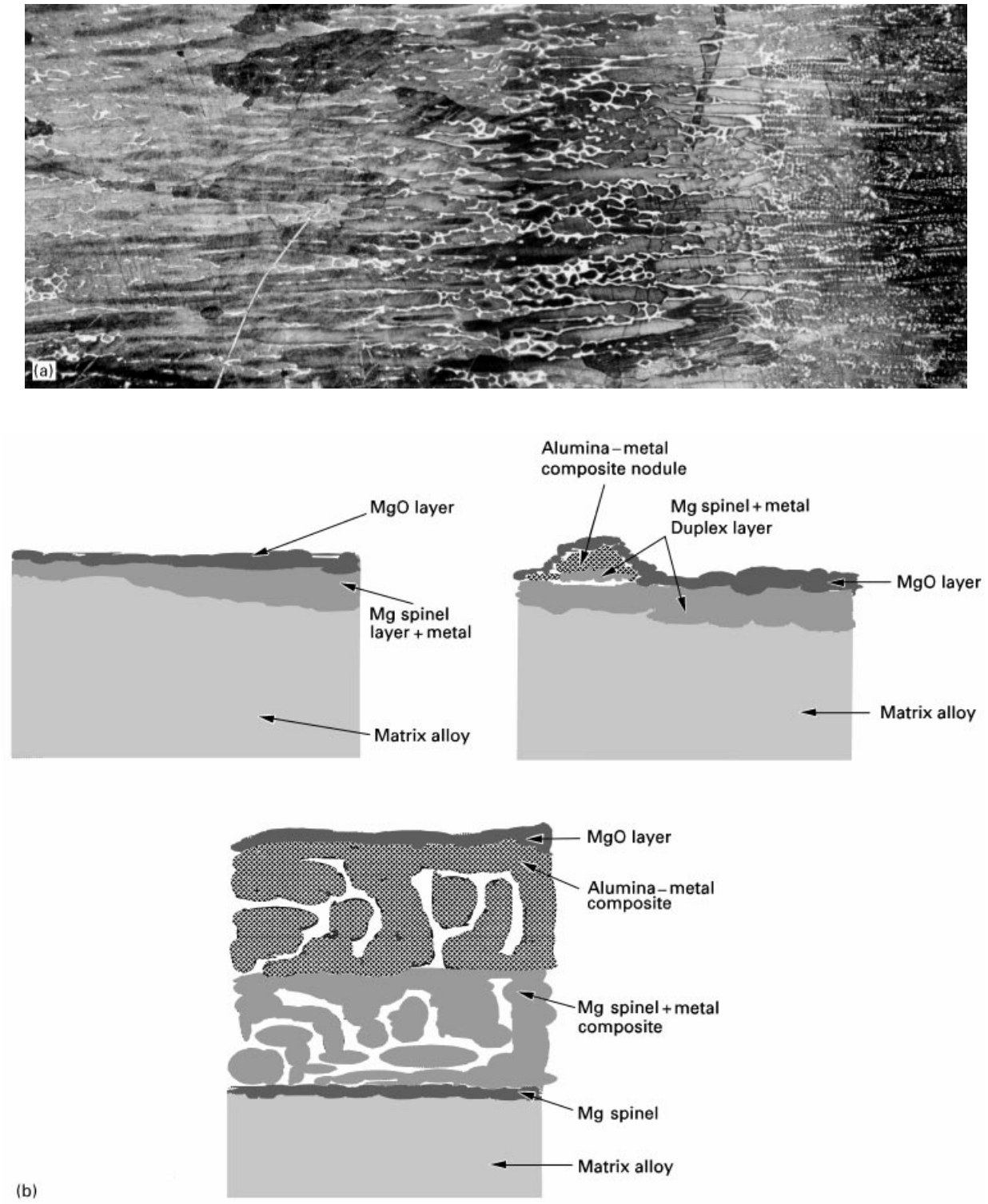

Figure 4 (a) Directionally solidified off-eutectic pseudobinary Ni–Al(–Cr) alloy showing aligned dual-phase microstructure [29]. (b) Schematic diagram showing different stages of structure evolution in Lanxide's self-infiltrated ceramic–metal composites [25].

alloying elements since composite growth is promoted by elements which form metastable surface oxides that prevent metal passivation. The composites produced using the other *in-situ* techniques (e.g., SHS) also show high porosity levels, and consolidation or infiltration is usually required to achieve full densification.

The *in-situ*-grown composites show clean interfaces, strong interfacial bonding, a uniform spatial distribution of particles and a narrow particle size distribution. Further structural changes are effected using secondary processes such as mechanical working, infiltration, and controlled solidification. For example, directional solidification of XD ingots of a Ti-43 wt % Al alloy containing 6 vol % (Ti, Nb)B randomly oriented short fibres led to a significant increase in the fibre length and aspect ratio together with axial alignment of the fibres along the growth direction. The boride phase dissolved during melting and resolidified as long fibres during directional solidification,

resulting in improved yield strength and flow stress [28]. In the case of melt-grown (arc-melted) buttons of γ-TiAl alloys containing Ta and B as alloying additions, a fibrous monoboride reinforcement phase forms with large (20 : 1) aspect ratio. The highly anisotropic growth of fibres from the melt results in improved creep strength of γ-TiAl. When the arc-melted alloy is remelted and splat quenched, a highly refined structure is obtained because the initial coarse rod structure dissolves and resolidifies as thin flakes in the interdendritic regions after splat quenching [30]. Other *in-situ*-grown composites and their structure have been presented in references [31–33].

4.3. Semisolid formed composites

Because an alloy containing a discontinuous ceramic reinforcement has low deformation resistance in the mushy state, it can be economically formed into net-shape components using forging, extrusion or die casting [34–37]. The semisolid forming processses overcome the problems of rapid tool deterioration and fracture of the reinforcement that accompany solid-state forming processes. The lower fabrication temperatures (typically 100 °C lower for Al) than conventional casting temperatures, reduced liquid metal handling, shape retention and easy transportability of the semisolid slugs, laminar flow during die filling (less porosity), lower solidification shrinkage (due to lower liquid content, typically 40%), and low deformation resistance of the mushy alloy due to globularization of the primary solid by coalescence, make semisolid forming a viable alternative to both traditional casting and metal-working techniques. Fig. 5 shows microstructures of a semisolid formed (compocast) Al–Si–Cu matrix composite containing slag particles. A small percentage of ceramic particulates modifies the dendritic structure, but a somewhat non-uniform distribution results. Higher particulate loadings lead to a more homogeneous particle distribution and a near complete transformation of dendritic structure to fine globular which coarsens with increasing holding time in the mushy state. The smaller interparticle spacings at high particulate concentrations restricts the growth and coarsening of the microstructure which results in finer globules [34]. The transformation of the structure from dendritic to globular is accelerated in the presence of particles compared with the unreinforced (rheocast) matrix alloy, possibly because the initial dendritic structure is finer in the composite and because a high dislocation density arising from the mismatch between the coefficients of thermal expansion of the matrix and the particles assists the process of recrystallization. The particles can then act as nucleation sites for recrystallized structure. Limited gravity segregation and particle clustering are observed in partially remelted composites after prolonged holding in contrast with fully remelted composites where appreciable segregation and clustering are observed [34]. The shearing action induced by vigorous stirring during particle incorporation also promotes globularization of the primary phase morphology which improves shear-induced flow behaviour. Semisolid

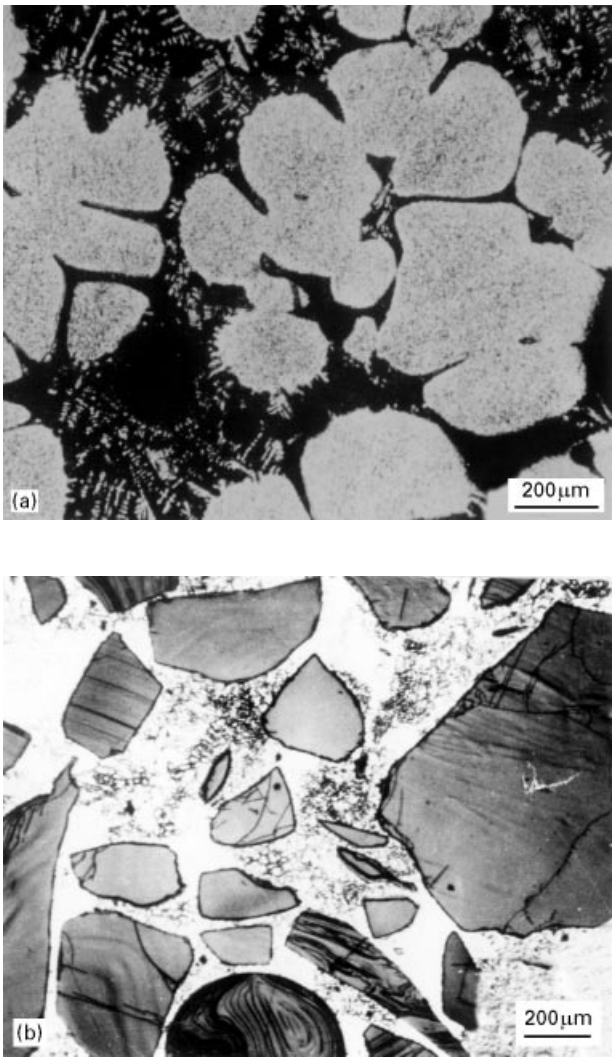

Figure 5 Microstructure of (a) partially solidified, vigorously agitated Al–Si–Fe matrix alloy, and (b) partially solid Al–Cu–Mg alloy containing slag particles from solid waste [35].

casting must be done at a temperature sufficiently high that enough liquid fraction is maintained but no degeneration of the globular microstructure or excessive chemical attack of the reinforcement by the melt takes place. The reinforcement resides in the interglobular spaces where the eutectic is associated with the reinforcement.

4.4. Centrifugal cast composites

Centrifugal casting is used both to position ceramic-enriched zones selectively within castings, as well as to generate centrifugal pressure for melt impregnation of suitably oriented fibrous preforms [38–42]. Particle segregation in pre-mixed suspensions during centrifugation is influenced by the particle size, pouring rate, metal temperature, rotational speed and heat transfer coefficient at the mould–metal interface (which can be varied using different mould coatings [39]). The cast structure consists of several microscopically distinct zones. With a boron nitride-coated mould, four distinct zones form radially in the unreinforced matrix alloy. Fast cooling near the mould walls results in very fine equiaxed primary dendrites whose size increases

radially towards the centre. Near the casting centre, columnar dendrites, aligned radially along the direction of heat extraction, form. In the immediate vicinity of the inside bore, an equiaxed dendritic structure forms owing to multidirectional heat extraction. When SiC particles are dispersed in Al, a thin particle-enriched region forms adjacent to the outer periphery owing to centrifugal force-induced segregation before the start of solidification. The adjacent zone retains the original particle volume fraction because high cooling rates do not permit particle rearrangement. The next zone, which is the actual reinforced zone, typically extends to roughly one third of the casting thickness in which particles are considerably segregated. Finally there is a particle-deduced dendritic zone with two distinct regions: a columnar dendritic zone and an equiaxed zone. In the reinforced region, solidification occurs rapidly, and no particle redistribution takes place. Particle distribution similar to the boron-nitride-coated moulds are obtained with graphite-spray-coated moulds.

The cooling rate is appreciably decreased with a Fibrefrax coating on the mould (which lowers the heat transfer coefficient at the mould–metal interface) and the dendritic structure is much coarser. The particle concentrations close to the maximum theoretical packing density of 52% can be achieved near the outer periphery. Sequential pouring of pre-mixed composite slurry and unreinforced matrix alloy in rotating moulds gives flexibility in positioning the reinforced zone at a desired location within the casting. Light particles (graphite, and mica in Al) segregate near the inner periphery, whereas heavy particles (zircon, and SiC in Al) segregate near the outer circumference of cast cylinders. The high concentration of particles in particle-enriched zones alters the solidification microstructure; for example, extensive shape modification of eutectic silicon is observed in particle-enriched regions of centrifugal castings of Al–Si–C composites [38].

4.5. Spray-formed composites

Spray forming combines rapid solidification of a fine dispersion of liquid metal droplets that impact a target (e.g., continuous fibres wound on a rotating mandrel) at high velocities which aids consolidation and densification of the deposited material [43–50]. Alternatively, the discontinuous particulates are co-injected with the metal spray, allowing particulate engulfment in molten or partially solid metal droplets either during flight, or upon high-energy impact over a conducting substrate. With judicious control of the operating process parameters, a homogeneous distribution and a fine grain structure are achieved both of which improve the fracture toughness and fatigue strength. The droplets in the spray are subjected to pressure forces which cause droplet disintegration under conditions where the dynamic pressure from gas velocity exceeds the cohesive forces (surface tension) which act to preserve the droplet integrity. The droplet velocity and volumetric concentrations are higher in the core region of spray cone than in the peripheral zones. Therefore, the relative velocity between the droplets and the carrier gas is small in the core region, and the thermal energy is large owing to higher droplet mass flux. This impairs the convective heat transfer from the droplet to the gas and leads to higher deposit densities in the core regions of the deposit. On the other hand, microstructure at the extreme surface of the deposit is dominated by powders that arrive nearly fully solidified. Thus, spatial variation in the structure of spray-atomized and deposited material is usually observed [49]. The as-deposited material in the peripheral zone shows a layered structure with deformed or fractured dendrites and prior droplet boundaries (Fig. 6a). On the other hand, droplets arriving in the core region of the spray cone show a fine spheroidal grain structure (Fig. 6b) because the solidification mode on the substrate is incremental (Fig. 6c). During incremental solidification, the rate of heat dissipation (by conduction through the deposit and the substrate, and by radiation and convection through the ambient gas) relative to the rate of spray deposition per unit area is such that a thin flm of liquid is maintained at all times on the deposit; as a result the impinging droplets meet the liquid film and the two liquids flow together before solidification occurs. This eliminates splat boundaries and yields a fine-grained equiaxed structure (Fig. 6b).

Solid nuclei begin to form within the droplets during flight, most notably in droplets in the outer (peripheral) regions of the spray, by processes of heterogeneous nucleation, surface nucleation, surface oxidation and interdroplet collision. The probability of achieving a high degree of undercooling before nucleation is high for smaller droplets. However, even for small droplets, the large undercoolings required for homogeneous nucleation may be impossible to achieve and heterogeneous nucleation will proceed at relatively lower undercoolings. The presence of particles in the droplets due to in-flight penetration of liquid or semisolid droplets will catalyse the heterogeneous nucleation; the solid dendrites then appear to emanate from the particle surface (Fig. 6d). The droplet penetration by particles must be completed before droplet solidification in order to achieve a homogeneous particle distribution. When tungsten and alumina particles (7–10 μm) were separately injected into a copper matrix spray, the W particles showed a uniform distribution in the deposit whereas alumina particles did not penetrate the copper droplets and were distributed inhomogeneously in the matrix.

When solidification is not completed in flight, a thin liquid film will be retained on the substrate surface after the arrival of the partially solidified droplet. The mechanical force of impacting will break the surface oxide layers on the arriving droplet as well as the pre-existing liquid film and will cause the dendrite arms to disintegrate into smaller segments. The fragmented dendrite arms would then lead to formation of an equiaxed grain structure via a grain multiplication mechanism. In addition, turbulent melt convection due to high-energy impact will assist dendrite root melting and detachment, causing grain refinement. Alternatively, particles may be mechanically entrapped in the solid during high-velocity impact

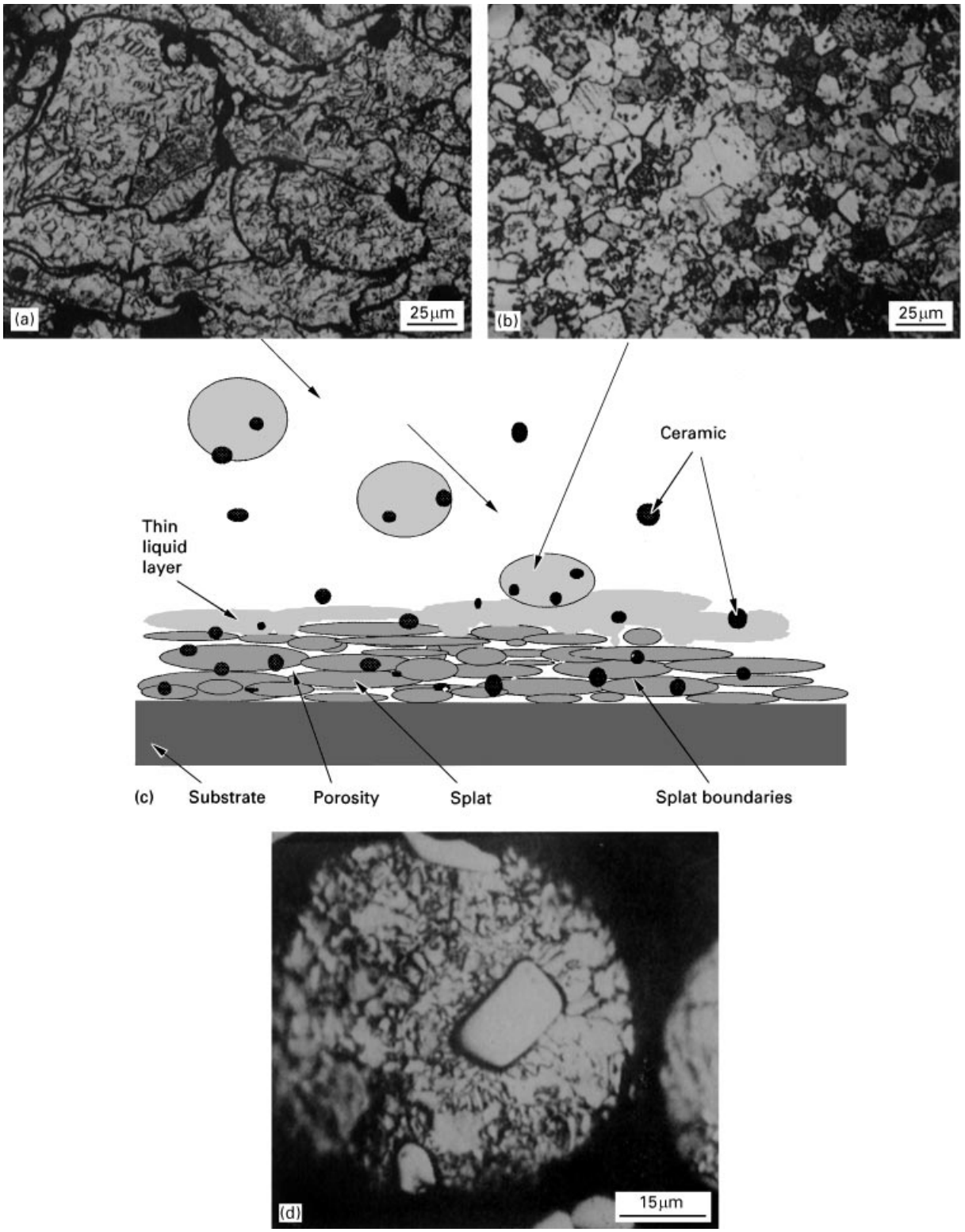

Figure 6 (a) A layered microstructure of as-deposted monolithic Ni_3Al from the outer regions of the spray cone, showing deformed and fractured dendrites, and thick prior droplet boundaries; (b) microstructure of Ni_3Al from the core region showing fine spheroidal grains; (c) schematic diagram showing mechanism of incremental solidification; (d) microstructure of spray-formed TiB_2–Ni_3Al composite showing heterogeneous nucleation on TiB_2 particles (a), (b) and (d) are from [43], and (c) from [46]).

(100–400 m s^{-1}). When a particle is incorporated in the solid by mechanical entrapment, the mechanism involves particle capture by multiple solidification fronts (Fig. 7) [44, 49]. As the fronts converge, a capillary region forms around the particle. Thus the particle is subjected to mechanical forces due to capillary action in addition to other forces such as repulsive surface forces from solidification fronts, and fluid convection resulting from impact and fragmentation processes. The combined effect of these forces is believed to push the particle out of the capillary region (smooth and isotropic particles are more likely to be ejected than rough particles with high aspect ratios). As the particle is displaced from its initial position, subsequent impact by an impinging droplet leads to engulfment.

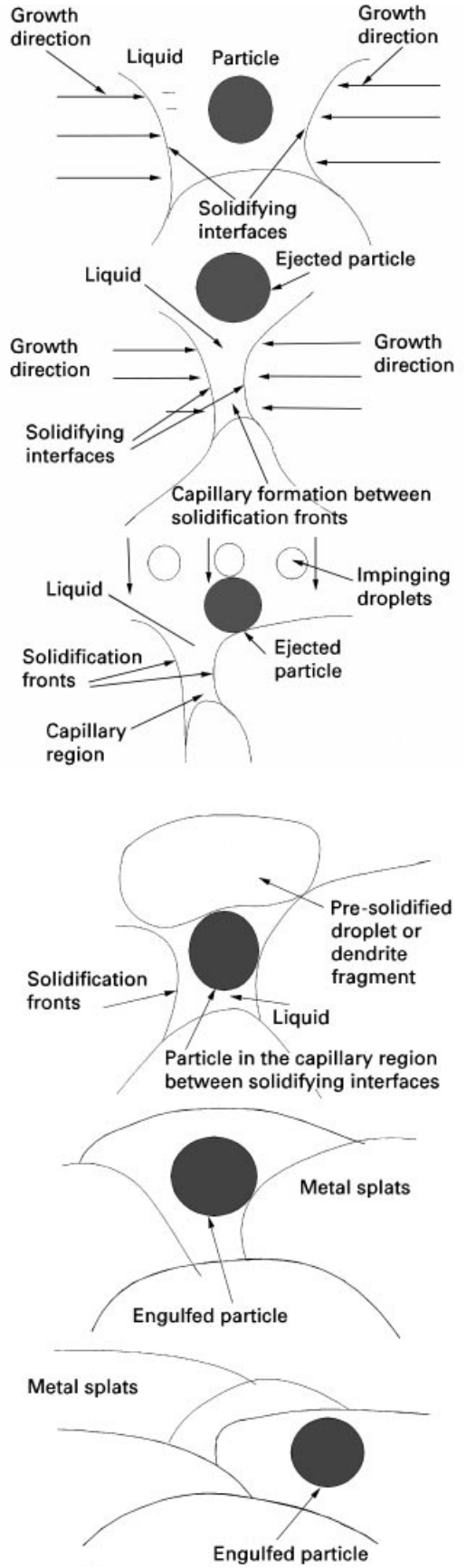

Figure 7 Particle entrapment in the spray formed material by mechanically driven entrapment [49].

The structure of the spray-formed material may exhibit featureless zones, splat boundaries and porosity, and cellular, dendritic or equiaxed zones depending upon the undercooling levels and growth conditions [49]. Fine atomized powders show featureless zones which are indicative of extensive solute trapping resulting from large solidification velocities. The porosity in the material is due primarily to interstitial effects (irregular cavities left in between impacting droplets), which is consistent with typical deposition conditions such as spray density, powder size and fraction solidified (porosity due to gas and solidification shrinkage is usually small). The porosity content of the deposits vary from the axis of the spray; porosity is higher near the outer periphery of spray cone than in the core regions, because of a larger proportion of pre-solidified droplets. Finally, the relatively short particle–matrix interaction times of spray forming are usually sufficient to cause near-interfacial changes and formation of stable chemical bonds (the embrittlement caused owing to large interfacial reaction product layes is avoided).

5. Porosity in cast composites

Apart from shrinkage that results from metal contraction during solidification, gas porosity presents a serious quality-related problem in cast composites. Common metals (Al and Mg) dissolve hydrogen in the molten state, and the supersaturation of liquid metal in hydrogen may cause nucleation and growth of gas bubbles which are entrapped during solidification [36, 37, 51, 52]. Gas may also be introduced owing to vigorous fluid shear as in stir-cast composites in which bubble suction, bubble coalescence and particle–bubble clustering lower the casting yield. The high fluid shear also leads to bubble disintegration into energetically more stable finer bubbles. Particle adhesion to fine bubbles decrease the bubble float-up rate and stabilizes gas in the melt. During solidification, the bubble–particle clusters are pushed into the last freezing eutectic colonies, forming interfacial porosity and weakening the interface. An optimum stirring rate allows bubble removal and particle retention. Pores could also heterogeneously nucleate on inclusions and particles during solidification [53]; particles act as barriers to fluid transport and solute diffusion. If the pressure drop between the front and the inclusion is large enough to overcome the fracture pressure of the bubble, the embryonic bubble at the point of nucleation ahead of the front will withstand the surface tension forces without collapsing (inclusions which are easily engulfed by the solid are not harmful as far as the nucleation of pores is concerned).

6. Nucleation and growth effects

During the solidification of discontinuously reinforced composites, the reinforcing phase suspended in the melt may serve as a preferred site for heterogeneous nucleation of primary phases crystallizing from the melt. Silicon is known to nucleate heterogeneously on the surfaces of C, Al_2O_3, silica and SiC; as a result, primary Si crystals in hypereutectic Al–Si alloys become partially refined [38, 54–65]. Direct additions of finely divided alumina with freshly formed surfaces are known to promote nucleation of Si. Similarly, in Al–Si–Ni alloys, where Ni enters the matrix as a result

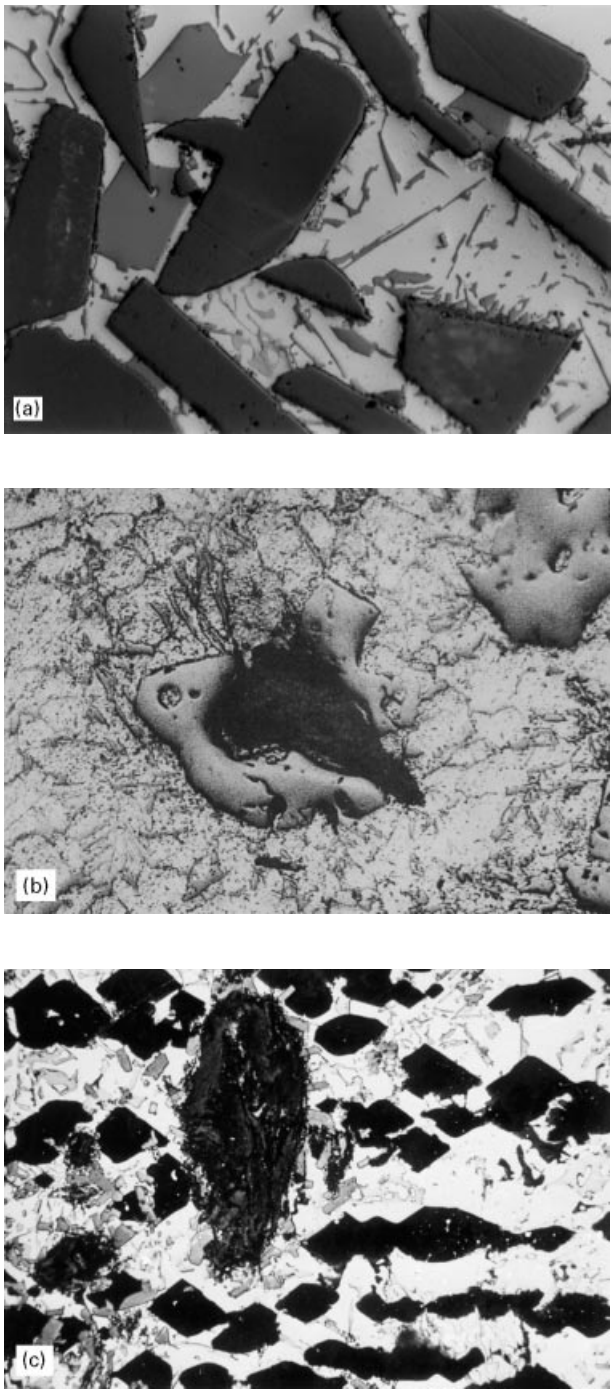

Figure 8 Photomicrographs showing the influence of dispersed particles on nucleation in the cast composites (a) SiC–(Al–Si) alloy, (b) graphite–(Al–Si) alloy and (c) graphite–(Al–Si–Ni) alloy [61, 62, 64].

of its dissolution from the surfaces of Ni-coated reinforcement, the intermetallic compound $NiAl_3$ nucleates on the particle [66, 67]. On the other hand, primary phase dendrites in several hypoeutectic Al, Zn and Mg alloys usually tend to avoid the dispersed particles [68, 69] and do not nucleate on their surfaces. As a result, the primary phase nucleates in the centre of interparticle regions and grows towards the particles so as to avoid the particles. The particles are therefore associated with the last freezing liquid where they modify the eutectic. Fig. 8 shows photomicrographs of some cast composites where the primary phase either nucleates on the particle surface or within interparticle regions.

The microscopic evidence of a phase initially nucleating on a particle may be obliterated because of convective transport of the particle to a higher-temperature region in the melt. If appreciable temperature differences exist between the particle and the melt, the nucleation of lower-melting primary phases (α-Al, α-Mg and α-Zn) might be unlikely; however, temperatures may be low enough to permit nucleation of higher-melting phases such as silicon and nickel aluminides. The crystallographic anisotropy of interfacial energies is also important; the reinforcing phase suspended in the melt may not be suitably oriented with respect to nucleating crystal to present a low-energy surface to it.

The modification of eutectic in Al–Si alloys from coarse acicular to fine spheroidized is accomplished by adding sodium, strontium, antimony or rare-earth elements to the melt. In the case of particulate-reinforced composites, the modification treatment can be carried out before particle dispersion in the melt because particulates dispersions do not appear to obliterate the modified structure [38]. In localized particle-enriched zones, the dispersed particles show some tendency to refine the structure; the particles, therefore, aid conventional modifiers and refiners such as sodium and phosphorus [64].

The grain refinement caused by heterogeneous nucleation during solidification is well known. It is, however, not always clear whether nucleation in a given situation is truly heterogeneous, i.e., whether a nucleus forms on pristine reinforcement surface or an intermediate transition layer (even a monolayer) first forms on the reinforcement to modify its surface energy and to improve its nucleation potency. Metals show widely different nucleation behaviours in the presence of ceramic reinforcements. The grain size of Al–4.5 wt % Cu is not affected by SiC or alumina, but reaction sintered porous TiC reinforcement (known to act as a heterogeneous nucleation catalyst for Al) reduces the matrix grain size by several orders of magnitude [55]. Similarly, heterogeneous nucleation of primary phases on carbon in Cu–Pb–Ti, alumina in Al–Cu–Ti, and TiB_2 in Ti–Al–Mn and Al alloys is well known [70, 71], although some controversy exists relative to the role of TiB_2 [72].

As matrix grain sizes appreciably larger than reinforcement size are also frequently observed in cast composites, it would appear that fibres do not assist primary-phase nucleation. However, besides heterogeneous nucleation, two other mechanisms of grain refinement must be considered. First, during composite fabrication using preform infiltration, the thermal interactions between cold fibres and hot metal could lead to rapid initial freezing of a thin sheath of solid onto the fibre; if the metal velocity and thermal conditions are such that the solid sheath does not remelt by the upcoming hot liquid, grain refinement will result [14, 55]. Second, in stir-cast composites, the insoluble solid particles increase the effective suspension viscosity and inhibit large-scale convection; as a result, grain refinement resulting from convective transport of dendrite fragments and solid nuclei could be suppressed. Hence, compared with an unreinforced

casting, a composite casting will show a greater tendency for columnar-dendritic solidification.

In the TiC–Al system, the TiC particles react with liquid Al to form carbides (Al_4C_3 and Ti_3AlC) which promote the nucleation of Al. On the other hand, both particle pushing without heterogeneous nucleation, as well as grain refinement are noted in sand and permanent mould-cast SiC–AZ91 Mg composites, and in directional solidified A356 Al–SiC_p composites [73, 74]. The measurement of undercooling from thermal analysis [73, 74] showed that the unreinforced AZ91 exhibited 0.9 °C undercooling for primary-phase nucleation, whereas the SiC–AZ91 composite did not show any undercooling. The as-cast structure showed the eutectic compound $Mg_{17}Al_{12}$ at the grain boundaries in both the composite and the matrix alloy casting; however, a finer grain size (42 μm) is achieved in the composite relative to the matrix alloy (127 μm) under identical casting conditions. In the absence of fluid flow effects, grain refinement results from two separate processes: rapid nucleation of new crystals and limited growth of nucleated crystals. Heterogeneous nucleation [75], if followed by slow growth, will lead to a situation where the final structure will show the grain-refining influence of particles. Limited solute diffusion during growth due to barrier effects of particles will probably restrict the growth; the delayed growth from the melt will give additional time for the formation of more nuclei. Both these processes will yield a refined structure.

Reactive elements promote wettability due to interface modification by transition layer formation which enhances heterogeneous nucleation and grain refinement. Thus, in the (Cu–Pb–Ti)–C composites, the α′ phase (30 wt% Pb, 15 wt% Ti and balance Cu) and the Ti_4Pb phase crystallize around the graphite particles [70]; both these phases form coherent interfaces with graphite. Similarly, in the (Al–Cu–Ti)–Al_2O_3 composites, the particles are surrounded by the $CuAl_2$ phase which also forms a coherent interface with the alumina. The measurements of solidification rates shows enhanced nucleation and growth in these composites relative to the base alloy. Similarly, in cast Al_2O_3–MgAl composites, a thin layer of primary Mg forms on the fibres [69]; the fibres induce nucleation because of rapid formation of spinels ($MgAl_2O_4$). Thus, selective incorporation of reactive elements will catalyse the heterogeneous nucleation provided that a low-energy intermediate transition layer is formed at the interface.

Conclusions similar to these are reached in droplet solidification experiments [76] in which heterogeneous nucleation in microscopically discrete melt droplet–reinforcement systems is investigated. When the subdivision of composite sample into a large number of droplets is achieved (e.g., with the use of a spray technique), a condition is reached in which each droplet contains on average only one reinforcement particle. By examining the cooling and solidification response of a collection of such reinforcement–droplet systems, the influence of reinforcement on alloy solidification reactions can be isolated. Al alloy droplets containing Al_3Ti inclusions clearly show a well-developed dendritic pattern emanating from the encapsulated particles, suggesting heterogeneous nucleation of α-Al [76] (for dendritic growth at contact angles less than 90°, the matrix will first grow in the shape of a continuous coating covering the particle surface from which secondary arms can grow outwards [7]). Similarly, stable metal oxides present a surface to the liquid matrix that is very much like the matrix oxide itself (e.g., Y_2O_3 in Sn droplets). On the other hand, oxide particles (e.g., PbO in Sn) which are less stable than the matrix oxide show a freezing behaviour indicative of a reduction reaction at the matrix–particle interface. These experiments suggest that melt–reinforcement interactions that are critical in determining the wetting and bonding need not involve gross chemical reaction layers but instead can be controlled by microscopic interactions that lead to near-interfacial changes.

The lattice disregistry between interfacing atomic planes of the substrate and the solid nucleus must be small for heterogeneous nucleation to take place. In the case of hypereutectic Al–Si alloys, primary silicon nucleates on dispersed SiC, indicating a favourable interface structure relationship. As $\alpha > 2$ for Si ($\alpha = L/kT$, where L is the latent heat, k is the Boltzman constant and T is the temperature), the silcon phase will grow in a faceted manner and form an atomically smooth interface with SiC. Silicon may form on SiC by a two-dimensional nucleation mechanism as long as there are coherent or semicoherent planes at the interface between the two. An orientation relationship of the type [63] $(111)_{Si}//(0001)_{\alpha\text{-SiC}}$; $[011]_{Si}//[1120]_{\alpha\text{-SiC}}$ will exhibit a relatively small mismatch of -6.9% when a match of three Si atoms in Si and every four Si atoms in α-SiC is considered [63]. The mismatch, Δ, is defined from $\Delta = (d_{Si}\text{-}d_{SiC})/d_{Si}$ where d_{Si} and d_{SiC} are the closest interatomic distances between Si atoms in this arrangement. The Si phase can also nucleate on the spinel phase $MgAl_2O_4$ which forms in Al–Si–Mg alloys containing SiC. An orientation relationship of the type $(111)_{Si}//(111)_{MgAl_2O_4}$ $[011]_{Si}//[011]_{MgAl_2O_4}$ will minimize the lattice disregistry. In this arrangement every three Si atoms match up with every four Al atoms with a mismatch of 1% along the three $\langle 011 \rangle_{Si}$-type directions. While these relationships suggest theoretically possible interface structures, high-resolution electron microscopy examination is usually necessary.

The structure length scales (cell size or secondary DAS) are altered at high concentrations of the reinforcement; at low concentrations the effects may be marginal (Fig. 9). For example, in the case of SiC contents up to 20 vol% in a Al alloy 6061 composite, the primary cell size at constant cooling rate is only marginally reduced compared with the unreinforced base alloy; the relationship between cell size d and the cooling rate, T, is of the form $dr^2 = k$, where the exponent a is in the range 0.32–0.38 for the unreinforced alloy and 0.36–0.38 for the reinforced alloy with 20 vol% SiC [60]. Similar power-law relationships apply to SiC–A356 and other composites. The ceramic reinforcement depresses the liquidus temperature relative to the unreinforced alloy at high cooling rates; the

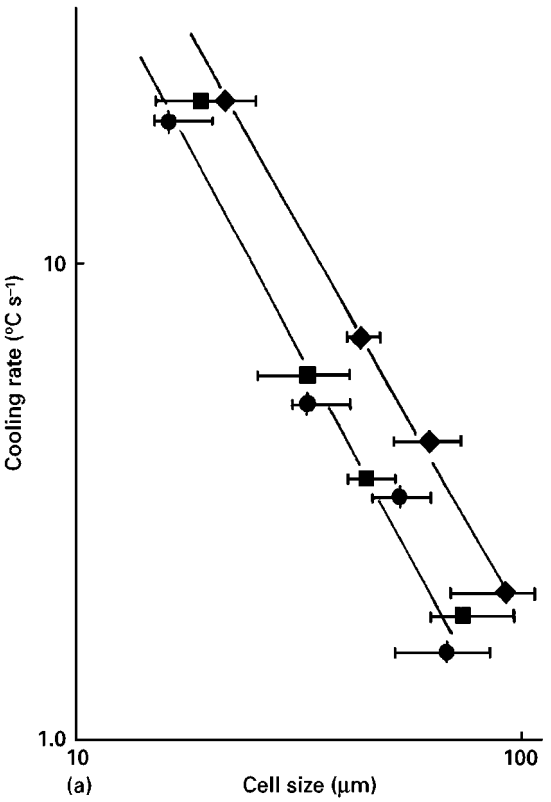

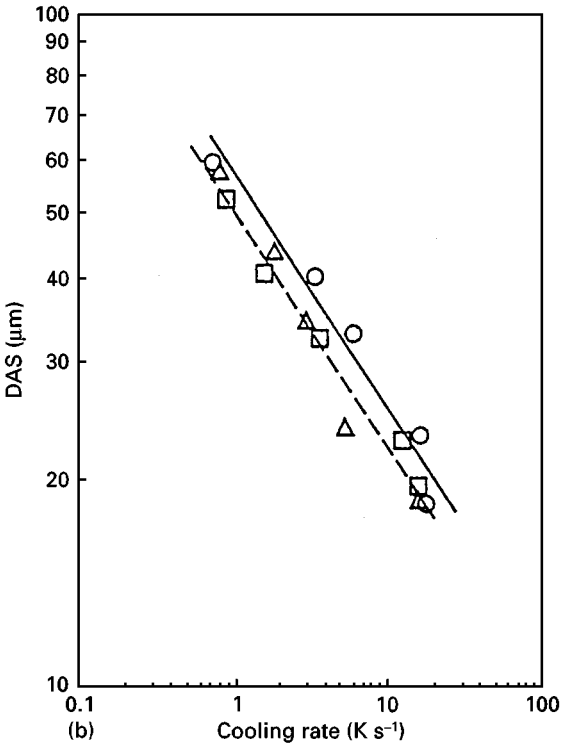

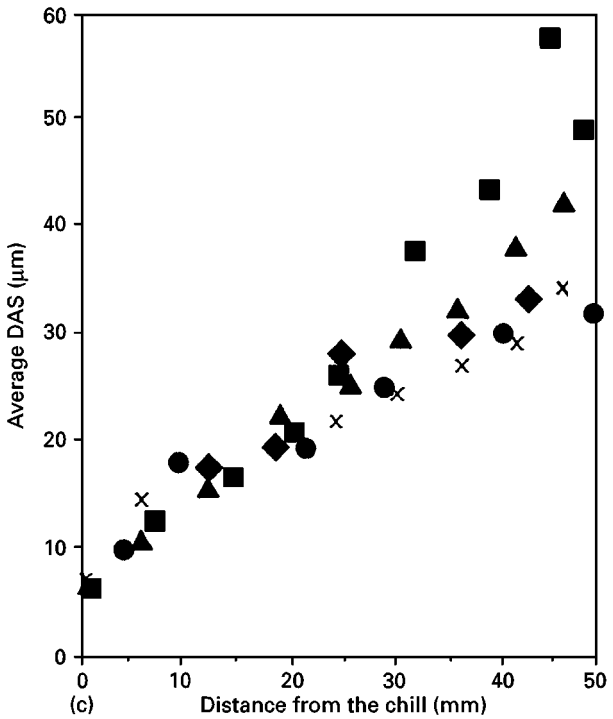

Figure 9 (a) Variation in cooling rate with cell size ((◆), Al alloy 6061; (■), Al alloy 6061–10 vol% SiC; (●), Al alloy 6061–20 vol% SiC) (b) Relationship between secondary DAS and cooling rate in some cast Al matrix composites ((○), A356; (□), (△), (- - -) composites) [60, 77]); (c) secondary DAS of SiC–(Al–Si) composites as a function of the distance from the chill ((■), 10 vol% SiC [78], (▲), 15 vol% SiC [78]; (◆), 20 vol% SiC [78]; (×), 0 vol% SiC [78]; (●) 15.5 vol% SiC [59]).

eutectic temperature is depressed more in the matrix than the composite [77, 78]. Also, the undercooling is smaller in composites and solidification time is greater in the unreinforced alloy in agreement with finite element calculations [80]. Finally, the ageing response of the composite could be impaired if the precipitation of certain phases (e.g., Mg_2Si in Al–Si–Mg) during solidification is suppressed because of consumption of reactive solutes (e.g., Mg) in interfacial reactions [81].

7. Particle distribution

When the melt–particle suspensions are held in the molten state for prolonged periods prior to solidification (e.g., during shape casting of remelted composite ingots), the discontinuous reinforcement tends to settle (or float) in the melt. Thus SiC and zircon settle to the bottom of the holding crucible, being heavier than Al [56, 78, 82–87]. The bottom sections of such castings show particle segregation, and upon prolonged holding, the top portions could be rendered particle-free. Similarly, light particles (mica and carbon in Al) float up due to their lower density relative to the metal [61, 88, 89]. Considerable clustering and network formation are also noted upon prolonged holding. Low temperatures increase the effective suspension viscosity, reduce particle settling and deflocculate particle clusters by shear; however, suspension fluidity must be sufficient to make defect-free composite casting. The processes of particle agglomeration, particle interactions with solidifying interfaces and fluid flow are all influenced by the Earth's gravity; these processes are altered, generally favourably, in the microgravity environment of space.

As particles modify and refine the structure, a non-uniform distribution produces spatial variation of structure and properties. Some control on particle distribution can be achieved by increasing the cooling rate, reducing the section thickness, or by using

microchill powders and water-cooled moulds [89]. Rapidly solidified (splat-quenched) composites show fine dendrites, reduced interdendritic segregation of particles, and a homogeneous particle distribution [84, 90]. The secondary DAS increases progressively with increasing distance from the chill (Fig. 9c). The particles are distributed more homogeneously in the immediate vicinity of the chill whereas the distribution becomes more inhomogeneous with increasing distance from the chill; the particles then tend to segregate at the intercellular region separated by the relatively coarse dendrites.

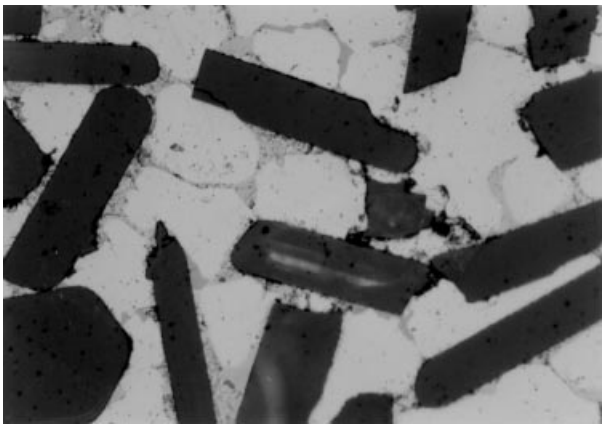

Figure 10 Photomicrograph showing the pushing of SiC particles in the last freezing eutectic colonies on an Al alloy [91].

8. Solidification morphology, particle distribution and particle pushing

The microscopic distribution of particulate reinforcement within the cast matrix is usually quite inhomogeneous, and the particles segregate into the last freezing interdendritic regions as a result of pushing by the primary solid (Fig. 10). The interdendritic segregation of particles is a serious quality-related problem in composites. Segregation causes severe agglomeration and interparticle contact and impairs the mechanical strength; segregation is most severe at small particle sizes and at large DASs [92, 97]. If the secondary arms are too closely spaced for a particle to fit in between them, then the particle is pushed by the entire dendrite.

The long-range solute interactions are perturbed by the particles. When a solidification front approaches a particle within a distance D/V of the particle (D is the diffusion coefficient, and V = the growth velocity), the particle begins to act as a physical barrier to diffusion of solute. This decreases the solute gradient and the local velocity of the growth front below the particle relative to the rest of the interface; the interface segment below the particle acquires a curvature which increases the lateral solute currents and accelerates the interface. However, the leading portion of the interface is soon decelerated as it moves ahead in the regions of a large positive temperature gradient in the liquid, and the rest of the interface catches up. During this process, a solute-rich band is left behind, which surrounds the particle (Fig. 11). For planar growth fronts, interface velocities are small and interaction distances, D/V, are large. On the other hand, dendritic interfaces have smaller interaction distances since the solute is rejected laterally into the interdendritic region; the deformation of a dendritic interface is smaller than that of a planar interface. Large particles and/or high particle volume fractions provide a much more effective barrier to solute diffusion. On the other hand, fine particles in relatively low concentrations do not provide effective solute screening so that the solute interactions between the particle and the entire interface are small.

Because of the solute screening effect of dispersed particles, the morphological stability of the solidification front is affected [94, 95]. As per the classical linear morphological stability theory, the stability of an interface is determined by (i) the concentration gradient at the interface, (ii) the conductivity-weighted average temperature gradient at the interface and (iii) the surface energies. For an infinitesimal sinusoidal perturbation of interface shape and small latent heat of fusion, the dominant effect of particles is to modify the concentration gradients at the growth front. It has been shown [94] that an initially cellular interface may be healed and become planar when a significant volume fraction of particles is present ahead of the interface. Conversely, a planar interface accelerating between particles may become non-planar. Likewise, at high particle concentrations, an initially dendritic interface can become cellular. Once a cellular interface has formed and the interface traps the particles, it may not readily change to a dendritic

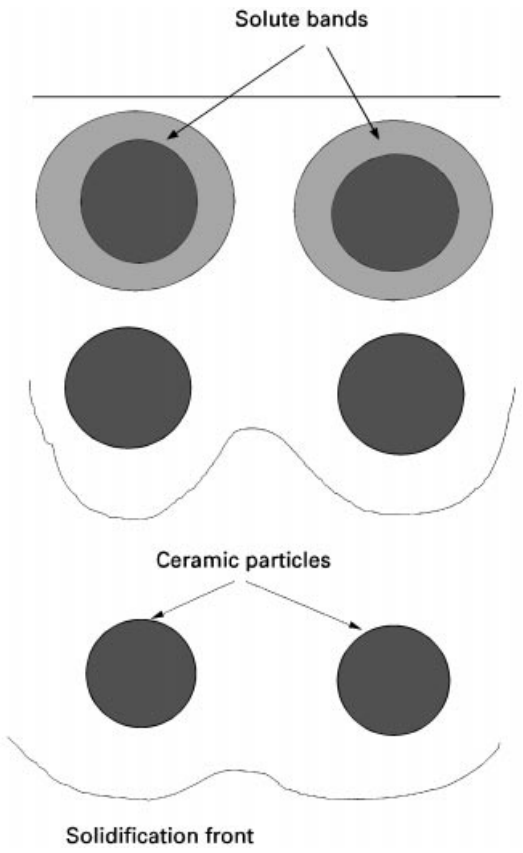

Figure 11 Schematic diagram showing solute banding resulting from interactions between dispersed particles and solidifying interfaces in alloys [94].

interface because the time required to readjust the solute diffusion fields could be large.

The dispersed particles could induce dendrite tip splitting [94] and deflect the local direction of crystal growth [96]. In the absence of particles, a unique stable dendrite tip radius is predicted by the theory as a result of balance between the destabilizing effect of solute gradients and stabilizing effects of capillarity. Thus, the conditions for tip splitting by the particles are determined by competition between these two factors. The particles ahead of the dendrite reduce the concentration gradient, G_c, which tends to stabilize the interface. For particles larger than the dendrite tip radius, the particles will exert a greater influence on solute gradient than on capillarity, and hence an initially dendritic interface will increase its tip radius, tending to become cellular. Conversely, very fine particles tend to reduce the dendrite tip curvature significantly, and tip splitting will occur as is observed in directional solidified transparent model systems [94]. Because particles tend to decrease the cell tip temperature,the length of the mushy zone and the extent of microsegregation will be reduced when a sufficiently high concentration of particles is present in the solidifying alloy. Besides morphological instability caused by particles, the geometrical entrapment between converging growth fronts must be considered. As particles induce morphological transitions and conversely, particle rejection and/or engulfment depends upon the morphology of the growth front, it appears that theoretical approaches to study particulate distribution should attempt to combine the morphological instability theories and particle-pushing theories.

The theoretical models of particle pushing predict the solidification conditions (e.g., growth velocity) which lead to a particular type of interaction behaviour (see [91, 98–100] for a summary of models). These models are based upon the fundamental assumption that surface energy provides the driving force for fluid transport into the gap between the particle and the solidification front (Fig. 12). In order for the particle to be pushed and the physical contact to be avoided, the thin liquid film between the front and the particle should not freeze. Thus, a balance between the repulsive interactions arising from the surface energy difference, and the attractive forces due to fluid drag which compresses the particle towards the front (and, therefore, favour engulfment) gives rise to a steady-state pushing configuration. Each of the theoretical models developed to date applies to some aspects of the phenomenon and explains some of the experimental data. The models differ from each other mainly in the mathematical sophistication (e.g., the boundary conditions that the solidification front must satisfy) and the method of solution but use a similar approach (e.g., balance of repulsive and attractive forces between particle and the front) to describe the process of interaction. In all the models, a zone of strong interactions between particle and the front is postulated; however, the dimensions of this zone (typically a few atomic diameters for the relatively short-range molecular interactions assumed in the models) are often based on parameters that are somewhat ill defined. In all the

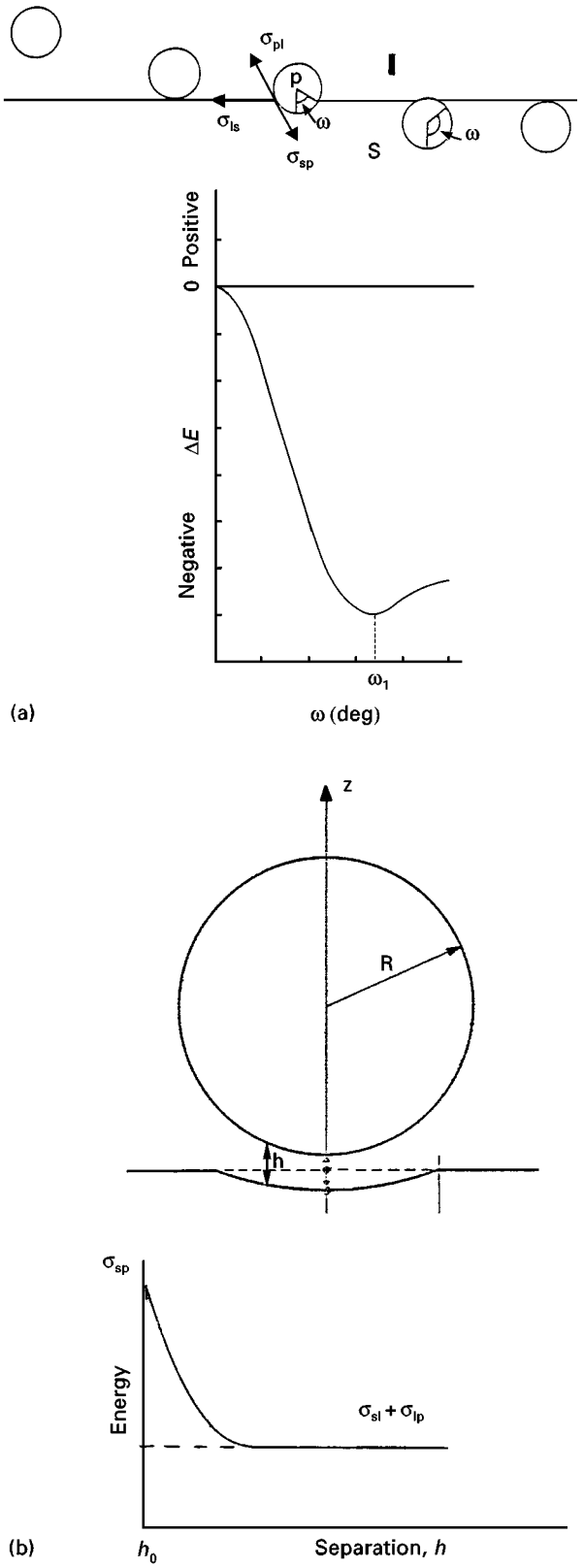

Figure 12 Diagram showing (a) particle pushing by a solidification front and (b) interfacial energy as a function of gap width between the particle and the front [91, 100].

models a well-defined critical velocity for pushing and/or engulfment transitions is calculated from a balance of attractive and repulsive forces, although sharp transitions in pushing and engulfment are seldom observed in real systems. Nevertheless, particle-pushing studies have shed considerable light on the role of material properties and process variables in the microscopic distribution of particles.

From a practical standpoint, the global cooling rate of a casting rather than the local growth velocity is a more readily accessible parameter, and particle-trapping criteria could be more meaningfully expressed in terms of cooling rate rather than critical growth velocity. The cooling rate also allows empirical determination of other microstructural features such as dendrite or cell size, whose relationship to the interparticle spacing is important in describing the segregation of particulates reinforcement. The applicability of this approach has been demonstrated in the case of TC–Al *in-situ* metal–matrix composites [101]. When the theoretical critical velocity for TiC capture by Al dendrites, calculated using the particle-pushing models, was converted to critical cooling rates (cooling rate equals the temperature gradient multiplied by the growth velocity) for various TiC particle diameters, the trapping behaviour observed in the experiments was found to be consistent with the theoretical predictions.

9. Other aspects of composite microstructures

The discussion in this article was confined mainly to microstructure evolution during the liquid-to-solid transformation of the fibre- and particle-reinforced alloys. The development of microstructure during post-solidification treatments is important to the development of final component properties. The ceramic reinforcements are known to modify the precipitation of phases during heat treatment and provide pinning sites for grain boundaries [101, 102]. For example, in alumina-reinforced Al–Cu alloys, the formation of Guinier–Preston zones is inhibited by the presence of fibres while the formation of Θ' precipitates is accelerated in the composite [102]. The segregation of solutes at the interface during ageing is altered by the reinforcement [103]. Microstructural changes associated with high-energy beam processes such as lasers include dissolution of reinforcement and precipitation of non-equilibrium phases [104, 105].

In summary, the solidification response of the matrix in cast composites is influenced by the insoluble ceramic reinforcement because the latter modifies the heat, mass and momentum transport processes, and the surface thermodynamics at the fibre–liquid–solid interface. As a result, the solidification kinetics, microsegregation and morphology of the crystals growing within finite-width channels between the reinforcement are altered. Solidification processing of metal-matrix composites has essentially evolved as a subset of the broad field of solidification of monolithic materials. It is now possible to design the composite microstructure through a judicious control of the solidification parameters.

Acknowledgements

An early draft of the paper was prepared at the Lewis Research Center, National Aeronautics and Space Administration (NASA), Cleveland, OH, with financial support from NASA and the National Research Council, Washington, DC. Appreciation is expressed to Thomas K. Glasgow, Chief, Processing Science and Technology Branch, Lewis Research Center, and S. N. Tewari, Professor, Cleveland State University, Cleveland, OH, for support and encouragement. Support received from the Universty of Wisconsin-Stout during preparation of the final manuscript is also gratefully acknowledged.

References

1. H. BOROFSKI, US Patent 2 170 259 (22 August 1939).
2. R. ASTHANA, *J. Mater. Synth. Process.* **5** (1997) 251, 339.
3. A. MORTENSEN, J. A. CORNIE and M. C. FLEMINGS, *Metall. Trans. A* **19** (1988) 709.
4. M. N. GUNGOR, J. A. CORNIE and M. C.. FLEMINGS, in Proceedings of the Symposium on Interfaces in Metal Matrix Composites, New Orleans, LA, March 1986 (Metallurgical Society of AIME, Warrendale, PA, 1986).
5. L. M. FABIETTI, V. SEETHARAMAN and R. TRIVEDI, *Metall. Trans. A* **21** (1990) 1299.
6. J. A. SEKHAR and R. TRIVEDI, in "Solidification of Metal Matrix Composites", edited by P. Rohatgi (Metallurgical Society of AIME, Warrendale, PA, 1990) p. 39.
7. A. MORTENSEN, *Mater. Sci. Engng.* **A173** (1993) 205
8. N. F. DEAN, A. MORTENSEN and M. C. FLEMINGS, in "Microstructure Formation in Solidification of Metal Matrix Composites", edited by P. Rohatgi (Metallurgical Society of AIME, Warrendale, PA, 1993) p. 83.
9. A. MORTENSEN, M. N. GUNGOR, J. A. CORNIE and M. C. FLEMINGS, *J. Metals* March (1986) 30.
10. D. G. McCARTNEY and J. D. HUNT, *Metall. Trans. A* **15** (1984) 983.
11. J. A. CORNIE, A. MORTENSEN, M. N. GUNGOR and M. C. FLEMINGS, in Proceedings of the Fifth International Conference on Composite Materials, edited by W. C. Harrigan Jr, J. Strife and A. K. Dhingra, (Metallurgical Society of AIME, Warrendale, PA, (1985) p. 809.
12. M. N. GUNGOR, J. A. CORNIE and M. C. FLEMINGS, in "Cast Reinforced Metal Composites", edited by S. G. Fishman and A. K. Dhingra (American Society for Metals, Materials Park, OH, 1988) p. 39.
13. G. GAGNON, K. K. CHAWLA, F. R. ARIA and B. ILSCHNER, *Z. Metallkde* **85** (1994) 5.
14. P. K. ROHATGI, C. S. N. NATH and D. WANG, in "Microstructure Formation in Solidification of Metal Matrix Composites"; edited by P. Rohatgi (Metallurgical Society of AIME, Warrendale, PA, 1993), p. 149.
15. M. A. KHAN and P. K. ROHATGI, in "Microstructure Formation During Solidification of Metal matrix Composites", edited by P. Rohatgi (Metallurgical Society of AIME, Warrendale, PA, 1993) p. 97.
16. A. MORTENSEN, V. J. MICHAUD and M. C. FLEMINGS, *J. Metals* Jan (1993) 36.
17. P. JARRY, V. J. MICHAUD, A. MORTENSEN, A. DUBUS and R. TIRAD-COLLET, *Metall. Trans. A* **23** (1992) 2281.
18. J. L. SOMMER and A. MORTENSEN, *J. Fluid. Mech.* **311** (1996) 193.
19. S. NOURBAKHSH, O. SAHIN, W. H. RHEE and H. MARGOLIN, *Metall. Trans. A* **22** (1991) 3059.
20. R. ASTHANA, S. N. TEWARI and S. L. DRAPER, *Metall. Mater. Trans. A* (1998) (in press).
21. M. M. KIM and F. E. GOODWIN, in "Squeeze Casting and Property Evaluation of Saffil-reinforced ZnAl Metal-matrix Composites" (Int. Lead-Zinc Research Organization, NC).
22. R. ASTHANA and P. K. ROHATGI, *Z. Metallkde* **84** (1993) 44.
23. E. MANOR, H. NI, C. G. LEVI and R. MEHRABIAN, *J. Amer. Ceram. Soc.* **76** (1993) 1777.
24. M. K. AGHAJANIAN, J. T. BURKE, D. R. WHITE and A. S. NAGELBERG, *Int. SAMPE Symp. Exhibit. Series* **34** (1989) 817.

25. S. ANTOLIN, A. S. NAGELBERG and D. K. GREBER, *J. Amer. Ceram. Soc.* **75** (1992) 447.
26. W. TANG and B. BERGMANN, *Mater. Sci. Engng* **A177** (1994) 135.
27. K. S. KUMAR, J. A. S. GREEN, D. E. LARSEN and L. D. KRAMER, *Adv. Mater. Proc.* **4** (1995) 35.
28. S. L. KAMPE, G. H. SWOPE and L. CHRISTODOULOU, *Mater. Res. Soc. Symp. Proc.*, **194** (1990) 97.
29. R. ASTHANA, R. TEWARI and S. N. TEWARI, *Metall. Mater. Trans. A* **26** (1995) 2175.
30. J. J. VALENCIA, J. P. A. LOFVANDER, J. ROSTER, C. G. LEVI and R. MEHRABIAN, *Mater. Res. Soc. Symp. Proc.*, **194** (1990) 89.
31. M. SINGH and D. R. BEHRENDT, *Mater. Sci. Engng* **A194** (1995) 193.
32. M. G. CHU and M. K. PREMKUMAR, *Metall. Trans. A* **24** (1993) 2803.
33. P. C. MAITY, S. C. PANIGRAHI and P. N. CHAKRABORTI, *Scripta Metall. Mater.* **28** (1993) 549.
34. M. A. BAYOUMI and M. SUERY, in "Cast Reinforced Metal Composites", edited by S. G. Fishman and A. K. Dhingra (American Society for Metals, Metals Park, OH, 1988) p. 169.
35. R. MEHRABIAN, R. G. RIEK and M. C. FLEMINGS, *Metall. Trans.* **5** (1974) 1899.
36. P. K. GHOSH, S. RAY and P. K. ROHATGI, *Trans. Jpn Inst. Metals* **25** (1984) 440.
37. V. LAURENT, P. JARRY, G. REGAZZONI and D. APELIAN, *J. Mater. Sci.* **27** (1992) 4447.
38. B. P. KRISHNAN and P. K. ROHATGI, *Metals Technol.* (1984) 41.
39. M. SUERY and L. LAJOYE, in "Solidification of Metal Matrix Composites", edited by P. Rohatgi (Metallurgical Society of AIME, Warrendale, PA, 1990).
40. D. NATH and P K. ROHATGI, *Composites* (1981) 124.
41. A. BANERJEE, P. K. ROHATGI and W. RIEF, in Proceedings of the European Materials Research Society Conference on Advanced Materials Research and Development for Transportation – Composites, Strasborg, November 1985, edited by P. Lamicq, W. J. G. Bunk and T. G. Wurm (Les Editions de Physique, Paris, 1985).
42. L. LAJOYE and M. SUERY, in "Cast Reinforced Metal Composites", edited by S. G. Fishman and A. K. Dhingra (American Society for Metals, Metals Park, OH, 1988) p. 15.
43. X. LIANG and E. J. LAVERNIA, *J. Metals* July (1993) 49.
44. T. S. SRIVATSAN and E. J. LAVERNIA, *J. Mater. Sci.* **27** (1992) 5965.
45. I. A. IBRAHIM, F. A. MOHAMMED and E. J. LAVERNIA, *ibid.* **26** (1991) 1137.
46. A. R. E. SINGER, *Mater. Sci. Engng* **A135** (1991) 13.
47. R. TEWARI, PhD Thesis, 1991, State University of New York, Stony Brook (1991).
48. A. LAWLEY and D. APELIAN, *Powder Metall.*, **37** (1994) 123.
49. E. J. LAVERNIA, *Int. J. Rapid Solidification* **5** (1989) 47.
50. S. SAMPATH and H. HERMAN, *J. Metals* July (1993) 42.
51. G. A. CHADWICK, *Mater. Sci. Engng* **A135** (1991) 23.
52. S. RAY, *Indian J. Technol.* **28** (1990) 368.
53. P. S. MOLHANTY, F. H. SAMUEL and J. E. GRUZELSKI, *Metall. Trans. A* **24** (1993) 1845.
54. M. K. SURAPPA and P. K. ROHATGI, *J. Mater. Sci.* **16** (1981) 983.
55. A. MORTENSEN and I. JIN, *Int. Mater. Rev.* **37** (1992) 101.
56. P. K. ROHATGI, R. ASTHANA and F. M. YARANDI, in "Solidification of Metal Matrix Composites", edited by P. Rohatgi (Metallurgical Society of AIME, Warrendale, PA, 1990) p. 51.
57. I. JIN and D. J. LLOYD, in "Fabrication of Reinforced Cast Metal Composites", edited by J. Masounave and F. G. Hamel (American Society Metals, Metals Park, OH, 1989) p. 107.
58. S. DAS, S. V. PRASAD, P. K. ROHATGI and T. R. RAMACHANDRAN, *Metall. Trans. A* **19** (1988) 1365.
59. A. KOLSGAARD, L. ARNBERG and S. BRUSETHANG, *Mater. Sci. Engng* **A173** (1993) 243.
60. D. J. LLOYD, *Compos. Sci. Technol.* **35** (1989) 159.
61. P. K. ROHATGI, R. ASTHANA and S. DAS, *Int. Metall. Rev.* **31** (1986) 115.
62. P. K. ROHATGI and R. ASTHANA, *J. Metals.* **43** (1991) 35.
63. W. WANG, F. AJERSCH and J. P. A. LOFVANDER, *Mater. Sci. Engng.* **A187** (1994) 65.
64. S. DAS, S. V. PRASAD, T. K. DAN and P. K. ROHATGI, in "Cast Reinforced Metal Composites", edited by S. G. Fishman and A. K. Dhingra, (American Society for Metals, Metals Park, OH, 1988) p. 243.
65. S. DAS, S. V. PRASAD, R. ASTHANA and P. K. ROHATGI, *Z. Metallkde* **80** (1989) 444.
66. F. A. BADIA and P. K. ROHATGI, *Amer. Foundry Men's Soc. Trans.* **79** (1969) 346.
67. S. ABRAHAM, B. C. PAI, K. G. SATYANARAYANA and V. K. VAIDYAN, *J. Mater. Sci.* **25** (1990) 2839.
68. M. A. DELLIS, J. P. KENSTERMANS, F. DELANNAY and J. WEGRIA, *Mater. Sci. Engng* **A135** (1991) 253.
69. FAZAL-UR RAHMAN, S. FOX, H. M. FLOWER and D. R. F. WEST, *J. Mater. Sci.* **29** (1994) 1636.
70. J. BRASZCZYNSKI, *Mater. Sci. Engng.* **A135** (1991) 105.
71. J. H. PERPEZKO, in "Metals Handbook", Vol. 15 (American Society for Metals, Metals Park, OH, 9th Edn, 1990) p. 101.
72. P. S. MOHANTY, F. H. SAMUEL and J. E. GRUZESKI, *Metall. Mater. Trans B* **26** (1995) 103.
73. A. LUO, *Scripta Metall. Mater.* **31** (1994) 1253.
74. B. INEM and G. POLLARD, in Proceedings of EUROMAT 91, Vol. II (Institute of Materials, London, 1992) p. 127.
75. M. C. FLEMINGS, "Solidification Processing" (McGraw-Hill, New York, 1974).
76. J. H. PERPEZKO, *Compos. Interfaces.* **1** (1993) 463.
77. S. GOWRI and F. H. SAMUEL, *Metall. Trans. A* **23** (1992) 3369.
78. P. K. ROHATGI, K. PASCIAK, C. S. NARENDRANATH, S. RAY and A. SACHDEVA, *J. Mater. Sci.* **29** (1994) 5357.
79. A. LABIB, H. LIU and F. H. SAMUEL, *Mater. Sci. Engng* **A160** (1993) 81.
80. S. HO and A. SAIGAL, *Scripta Metall. Mater.* **31** (1994) 351.
81. H. RIBES, M. SUERY, G. L'ESPERANCE and J. G. LEGOUX, *Metall. Trans. A* **21** (1990) 2489.
82. AXEL KOLSGAARD, DR.ING. Dissertation, University of Trondheim, The Norwegian Institute of Technology (1993).
83. M. GALLERNEAULT and R. W. SMITH, in Proceedings of EUROMAT 91, Vol. 1 (Institute of Materials, London, 1992) p. 205
84. P. K. ROHATGI, F. M. YARANDI, Y. LIU and R. ASTHANA, *Mater. Sci. Engng.* **A147** (1991) L1.
85. Y. WU, H. LIU and E. J. LAVERNIA, *Acta Metall. Mater.* **42** (1994) 825.
86. D. J. LLOYD, Proceedings of Symposium on Advanced Structural Materials, Edited by D. S. Wilkinson (Pergamon, Oxford, 1988) p. 1.
87. A. BANERJEE, M. K. SURAPPA and P. K. ROHATGI, *Metall. Trans. B* **14** (1983) 273.
88. A. K. JHA, R. ASTHANA, T. K. DAN and P. K. ROHATGI, *J. Mater. Sci. Lett.* **6** (1987) 225.
89. D. NATH, R. ASTHANA and P. K. ROHATGI, *J. Mater. Sci.* **22** (1987) 170.
90. N. J. FEI, L. KATGERMAN and W. H. KOOL, *ibid.* **29** (1994) 6439.
91. R. ASTHANA and S. N. TEWARI, *Processing Adv. Mater.* **3** (1993) 163.
92. J. W. McCOY and F. E. WAWNER, in "Cast Reinforced Metal Composites", edited by S. G. Fishman and A. K. Dhingra (American Society for Metals, Metals Park, OH, 1988) p. 237.
93. L. KURIAN and R. SASIKUMAR, *Acta Metall. Mater.* **40** (1992) 2375.
94. J. A. SEKHAR and R. TRIVEDI, *Mater. Sci. Engng* **A147** (1991) 9.

95. J. A. SEKHAR, R. TRIVEDI and S. H. HAN, in "Solidification of Metal Matrix Composites", edited by P. K. Rohatgi (Metallurgical Society of AIME, Warrendale, PA, 1990) p. 21.
96. L. YAOHUI, H. ZHENMING, L. SHUFAES and Y. ZHANCHO, *J. Mater. Sci. Lett.* **12** (1993) 254.
97. S. RAY and P. K. GHOSH, in "Solidification of Composites", edited by P. Rohatgi (Metallurgical Society of AIME, Warrendale, PA, 1990).
98. D. M. STEFANESCU, A. MOITRA, A. S. KACAR and B. K. DHINDAW, *Metall. Trans. A* **21** (1990). 231.
99. D. SHANGGUAN, S. AHUJA and D. M. STEFANESCU, *Metall. Trans. A* **23** (1992) 669.
100. R. ASTHANA and S. N. TEWARI, *J. Mater. Sci.* **28** (1993) 5414.
101. M. FERRY, P. R. MUNROE and A. CROSKY, *Scripta Metall. Mater.* **28** (1993) 1235.
102. L. PARRINI and R. SCHALLER, *Acta Metall. Mater.* **43** (1995) 1387, 2149.
103. M. STRANGWOOD, C. A. HIPPERLY and J. J. LEWANDOWSKI, *Scripta Metall. Mater.* **24** (1990) 1483.
104. K. M. JASIM, R. D. RAWLINGS, R. SWEENY and D. R. F. WEST, *J. Mater. Sci. Lett.* (1992) 414.
105. N. B. DAHOTRE, T. D. McCAY and M. H. McCAY, *J. Appl. Phys.* **65** (1989) 5072.

Received 13 May 1996
and accepted 12 November 1997